A 3D Processing Technique to Detect Lung Tumor

Nabila Elloumi[1], Hassan Seddik[2], Slim Ben Chaabane[3], Tounsi Nadra[4]
Phd Student, Electrical Engineering-University of Carthage-Computer Engineering Department-Tunisia Electrical Engineering University of Tunis-RIFTSI Research Laboratory-Tunisia-Biomedical Technician, Salah Azaiez Institute Tunis, Tunisia[1]
Professor, Electrical Engineering-University of Tunis-Tunisia, RIFTSI Research Laboratory, Tunisia., Tunis, Tunisia[2]
Assistant Professor, Faculty of Computers and Information Technology-University of Tabuk, Tabuk 47512, Saudi Arabia
Electrical Engineering University of Tunis-Tunisia, RIFTSI Research Laboratory, Tunisia[3]
Radiophysicist, Salah Azaiez Institute, University Tunis El Manar-Faculty of Medicine of Tunis, Tunisia[4]

***Abstract*—In this paper, the authors introduce a new segmentation technique based on U-NET algorithm from the deep learning used for lung cancer segmentation, which is the main challenge that medical Staff confront in their diagnosis process. The goal is to develop an ideal segmentation that enables medical personnel to distinguish the various tumor components using the completely U-NET convolution network architecture, which is the most effective. First, the regions of interest (ROI) in the 2D slides are established by an expert using the syngovia application of the Siemens. In this pre-processing step, the cancer area is isolated from its surroundings, and is used as a training model for U-NET algorithm. Second, the 2D U-NET model is used to segment the DICOM images (Digital Imaging and Communications in Medicine) into homogeneous regions. Finally, the post processing step has been used to obtain the 3D CT scan (computerized tomography) from the 2D slices. The segmentation results from the proposed method applied on biomedical images from nuclear medicine and radiotherapy that are extracted from the archiving system of the Institute of Salah Azaiez from Tunisia. The segmentation results are validated, and the prediction accuracy for the available test data is evaluated. Finally, a comparison study with other existing techniques is presented. The experimental results demonstrate the superiority of the used U-NET architecture applied either for 2D or for 3D image segmentation.**

***Keywords*—Deep learning U-NET architecture; 3D CT scan (computerized tomography); DICOM images (Digital Imaging and Communications in Medicine); 2D slices; ROI (regions of interest)**

I. Introduction

Some of the main difficulties in image processing and computer vision could involve split imaging [1]. The divisions of the imaging in just this topic have the broadest use across several disciplines and technical advances [2 and 3]. The most known concept is to implement different software for the feature spaces of both the partitioned 3D melanoma illustration and the U-NET measurement, in either the permitted dimensional characterizing boundary. Which the distributions produced with peak contribution through one pixel to the following juxtaposition. As well as a wide range of intensity only within the visual performance of the segment. The main idea is to create an optimum cluster approach with medical scanning ground and to obtain the wanted findings through analysis.

For medical images, only several segmentation methods are available [4, 5, 6, and 7]. Mohamed et al. [8] established that computed tomography (CT) imaging is one of the crucial development radiological aspects for illness diagnoses. In this study, the author provides an approach for CT image processing that integrates the spatial and transform domains. Low-contrast details that are often smoothed out by edge detection filters can be restored with the help of transform domain filters. The homogeneity Phase (PC) and the redesigned remove noise technique form the foundation of the prefilter. In the same context, Imen et al. [9] suggests a computer-aided diagnostic (CAD) method for diffusion-weighed magnetic resonance imaging (DWI)-based early identification of prostate cancer. That was defined as the region of interest for the proposed system across the several slices of the input DWI volume. The defined ROI appear the diffusion coefficient (ADC) which was determined, normalized and improved.

In order to identify local scale nodules less than 3 mm and non-nodules on tomography (CT scan) networks, Monkam et al. [10] has mentioned various CNN layouts also with many of convolution layers. The researchers were using a 5-fold parallel validation approach to assemble the designs on different shapes of (16×16) , (32×32) and (64×64) CT scan images captured from the LIDC repository at (512×512) . The experiments have found that the CNN with two fully connected layers within the instance of (32×32) patching, measure an incredible performance and prospective.

Similarly, Mundher Shabiet al. [11] researched a 3D convolutional neural network (CNN) established on the most important objectives. For the automatic recognition of the whole disease of lung cancer that is screened on computed tomography (CT) scans. If it can accurately classify malignant/cancerous lung nodules, many lives could be saved. In the meantime, SiyuanTangetal [12] explored the pulmonary tissue area and used a 3D U-NET convolution neural network.

Unfortunately, the outcomes of the preponderance extraction feature in practice when it is used on 3D medical data are erroneous. The fragmentation of lesions allows swift and exact disease identification by healthcare experts. Consequently, selecting the appropriate feature is an essential step in the analysis technique of a medical image.

The U-NET architecture is a particular sort of fully convolutional network (FCN) defined by an encoder-decoder structure. Those are developed for semantic segmentation, which is often referred to as pixel categorization. That was

developed for the direct extraction of high-level image from blocks during the expansion phase. These connections defined the block boundaries during the rectification.

Section 2 introduces the proposed method for detection of Lung Tumor. The experimental results are discussed in Section 3.The discussion is presented in Section 4 and the conclusion and future work is given in Section 5.

II. Proposed Approach

Forty cases were involved in the investigation (thirty males and ten females), with a prognosis and reported age range of 55 years (45-65 years). The cancerous nodule that was identified reached approximately 3 cm. Data extracted from the local system of storage and transfer of data (PACS) is extracted according to Salah Azaiez Institute of Cancerology various nuclear medicine, radio-assistance and radiotherapy in order to develop the optimization techniques. That approach out 3D lung cancer tiny cellular (CPC) of the multiple levels which would be associated with smoking use and contributes for 25% of carcinoma [15]. The non-small cell lung cancer (NSCLC) subgroup provides for the remaining 75% of cases of pulmonary cancer. The outcome displays the inadequate CT SCAN performance of seventeen patients.

In an attempt to evaluate the provided framework's efficiency, accuracy and awareness for the split samples, the consequences are juxtaposed against approaches that have been established as effective. Those protocols have been implemented on Ubuntu by using the deep learning framework and NumPy dialect settings.

The underlying 3D data is saved in the RGB (red, green, and blue) layout. The primitive shade occupies 8 bits per pixel, and the luminance can vary from 0 to 255. The engagement in learning how to tag the DICOM data will later be used for edge detection. The full-size cut with a measurement of (256×256) and an estimate of $(96 \times 128)$of the ROI is defined (see Fig. 11).

The Different diagnoses, which use a wide range of techniques to treat extended pathologies, are particularly employed on clinical imaging. With this field in healthcare, training is now immediately accessible. The medical techniques of imagery allowed a visual description focused on physical or chemical features instead of a straightforward snapshot of the tissue or organ being researched; especially those employed in nuclear medicine, which carry out reconstructive and volumetric acquisitions directly.

Consequently, the findings of the preponderance of the widely employed feature extraction, whenever extended to 3D medical data, are not consistent anymore. The major objectives are to make it simpler for clinicians to immediately and accurately diagnose malignancies. Therefore, among the most necessary phases in image processing is determining an optimal decision.

In this case, applying the U-NET approach to divide a three-dimensional image of a patient suffering from lung cancer seems like an intriguing technique. Therefore, the primary objective of this study is to develop the best algorithm. The biomedical engineering produces the desired optimal result for healthcare experts.

Preprocessing, U-NET segmentation and post processing are the three main phases that make up the proposed method. In the first phase, the local region of interest (ROI) and 3D volume have been converted into an arrangement of 2D slices in the first phase. The local area of interest is partitioned by using 2D U-NET framework in the second phase. Finally, the 3D CT SCAN has been reduced again to 2D slices by using the post-processing phase. The flowchart depicted in Fig. 1 demonstrates the characteristics of the proposed segmentation technique the contribution applied by extracting the different parameters from the syngovia system (the archiving system) in the input to the pre-processing, U-NET architecture, post-processing and the output result to obtain the 3D U-NET segmentation.

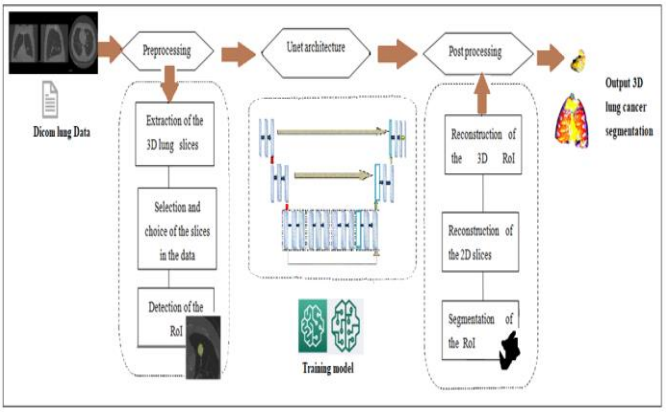

Fig. 1. Suggested approach defined by the preprocessing step the U-NET architecture and the post processing step.

The proposed algorithm of the U-NET can be summarized by the following steps:

Step 1: The 3D volume was changed into 2D slices, and the local Region of interest (ROI) was selected, which represents the ground truth an estimate of (96×128).

Step 2: Convolution layers, three - dimensional up-convolutions and 3D max partitioning -3D operations that substitute the professional 3D decompositions and thus are epitomized in 3D axes that are explored.

- The architecture involves screening out the highest-risk malignant nodule prospects among storage containers.
- The U-NET CNN architecture is a great tool for the segmentation of biomedical imagery. The recommended implementation of U-NET is the least straightforward way to reduce memory consumption; check Fig. 3.

For the training stage, the suggested U-NET adapted framework(256×256) as provided 2D Tomography scans are slices up and provided with information and annotation, as (256×256) overlays, and tumor regions are 1 while other regions are 0.

Step 3: The post-processing algorithm requires frames (256×256), in which each pixel's datatype ranges

from zero to 1, reflecting the likelihood that pixel is a participant. Fig. 2 to 4 illustrates identical entries and prognostications for all patients in the ultimate U-NET layer.

In this contribution, the U-NET strategy will be applied for the segmentation of the lung DICOM image. In this proposal, the authors begin with the preprocessing and the post processing. At the first stage, the 3D volume has been changed over into a course of actions into the 2D slices and the (ROI) has been made. At the second stage, the 2D U-NET demonstrates the utilized section nearby the ROI. Finally, the post processing step has been obtained to diminish the 3D CT SCAN from the 2D.

A. Pre-processing Procedure of 3D Lung Cancer Slices

The segmentation of the CT SCAN data is performed using the pre-processing approaches. To accomplish this frame, the 3D CT SCAN provided from the 2D slices must initially be stripped whereby each subject includes about 260 slices. Secondly, the 2D determined slices have been applied to establish the region of interest (ROI). The multi-view split of the crucial, coronal, and sagittal planes (see Fig. 6), has been performed by using deep learning techniques (the information of standardization and expansion).

The pre-processing steps convert the 3D CT SCAN into 2D slices in order to create the ROI, which could be used as an input by the 2D split. In an attempt to apply digital competence in a slice-wise strategy for greatest performance the 2D slices were produced from 3D slices. Those slices are obtained concurrently and applied at the orthogonal planar 3D in space, and the basic computing CDA was developed exclusively for DICOM imaging [13]. For the medical establishment, the authors opt for Siemens Healthcare that is specialized on PACS Syngovia software and is applied to the process of the 3D image segmentation expertise. This application is used to extract features of the DICOM images for the preservation and accomplishment support of a precise and efficient diagnostic.

In this location, the volumetric sampling adds a third dimension relative to two dimensions (2D) computerized in the following figures. The screening method is focused within the building blocks referred to as three-dimensional (3D) pixels. However, the volume rendering is made possible by the representation of (3D) datasets. Consequently, multidimensional components of numeric or data vectors are used to characterize the datasets. That is used to create the 3D CNN architecture that combines subsample and recorded values [14]. Fig. 2 illustrates the preprocessing steps in the beginning the choice of the appropriate 3D lung cancer that was extracted by the medical expert and selects the best slices to be used in the terminologies of the 2D slices and finally the different parameters was defined to obtain the appropriate ROI.

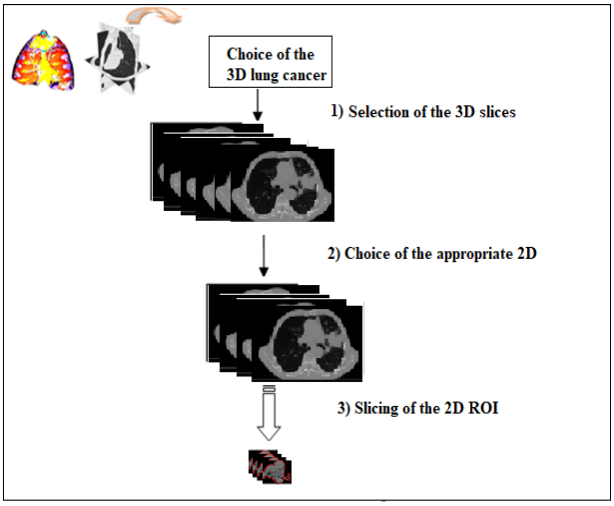

Fig. 2. Preprocessing step demonstrated by the choice of the 3D lung cancer. (1) selection of the 3D slices. (2) choice of the appropriate 2D. (3) slicing of the 2D ROI.

In order to be precise, the different parts of the slices have been resized to achieve the same (256×256) pixel approximation. This methodology decreased the number of 260slices presented as abnormal for every CT scan. Each procedure decreased the median slice count to every Scan between 260 into 35 (see Fig. 3).Consequently, the screened slices were subsequently projected on the region of interest (ROI), which had been extracted from the full-size cut with a measurement of (256×256) and an estimate of (96×128) as demonstrated in Fig. 3.

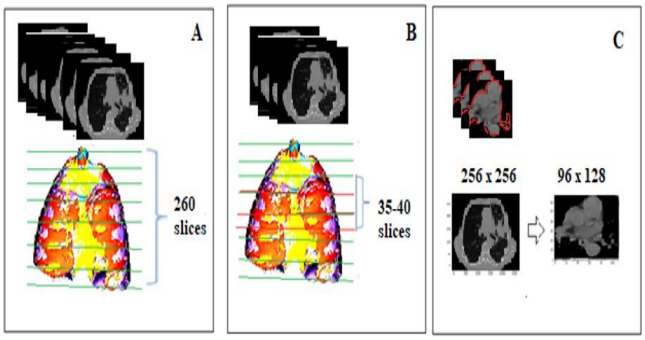

Fig. 3. Preprocessing steps, (A) the 3D slicing, (B) the selection of slices and (C) the region of interest (ROI).

B. 3D Extension based on 2D Segmentation using U-NET Architecture

The proposed method is employed from deep CNN and the data was implemented to stretch the 3D segmentation volume and have the latest new U-NET architectural decision. Fig. 4 contains the fundamental concepts of the segmentation applied to the U-NET configuration.

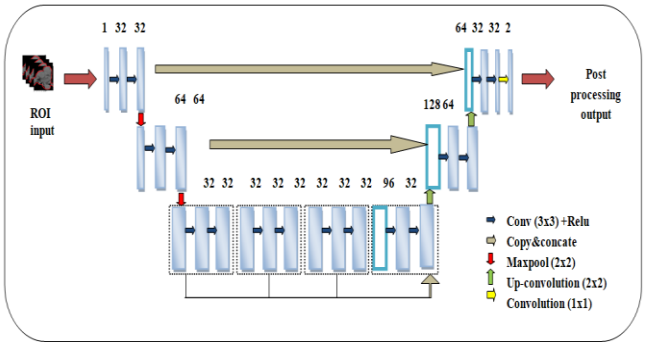

Fig. 4. The U-NET architecture approach presented by the input of the patched ROI into the defined layers and the output of the post processing step.

Regarding the difficulties of splitting in the medical field, it has been proposed that the U-NET approach presented as wide multilayer perception for this division process [15]. This expert system is one of the most well-suited and sufficient for partitioning clinical imagery. The approach made it possible to identify valuable details from DICOM. This technique includes an encoder and a decoder that accomplishes down, and up sampling using four components and are related via skip associations to produce high-resolution image.

Whilst also reducing the final two layers of the first explanation and boosting the bottleneck layer of the division result, the authors reduce the segmentation approximation under this project to 50%. By skipping connections, the characteristics acquired through the encoders' method at each level are transmitted to the decoding method. The encoder approach conducts two rounds of convolution, aggregate equalization, and dropout simultaneously for each layer. The image measurement will be split in half by the max-pooling and sent to the next layer. This handle is retained until the image reaches the bottleneck layer, the last layer in the encoder path. This layer now has three empty squares and two convolutional rounds that were normalized and discarded separately.

After the subsequent phase, the authors combined the yield from all previous blocks into the final bottleneck layer square. This experimentation with different amounts of blocks inside the hidden layer demonstrated of the three additional square configurations. The decoding path starts at the end of the pre-processing step on the upper right. The image identification is first expanded by the use of over fitting. Typically, a transposed convolution takes the place of the convolutions in oversampling. The image is then transmitted to the layer in the decoder method, which combines the highlight mapping from the contraction method (encoder), does two rounds of convolution group normalization, and independently performs dropout. The method continues sampling the images until each one approach the last stage of the decoder, at which point information is returned towards its original estimate of(96×128). The final layer of the decoding technique comprises a sigmoid stage that divides every pixel into two main categories with a probability ranging from 0 to 1.

According to Fig. 4, the image data is coupled to a rectangle size width (3×3)in order to generate a boundary inside the convolution implementation. For this reason, the authors use the ReLU actuation technique in each of these convolution patterns [16]. The positive weights of the attributes remained undamaged by this implementation process strategy, however all of the spotlights' deleterious evaluations have been assigned a value of zero.

Furthermore, Cluster standardization was employed to speed up the arrangement processing by decreasing the rate at which each gradient was received. The distribution changes during preparation since the characteristics of the previous time step change. Likewise, over fitting and Dropout are anticipated using the premature ceasing [17] as batch normalization tactics within the implementation. At every layer, the weight and inclination were improved using the Adam optimizer [18]. The ROI image of a slice from a cell lines CT SCAN serves as the input and the yield is the segmentation.

This solution performs well for connecting the intra-slice images, identifying the boundaries, and fragmenting the layers from the human lung CT SCAN dataset since the U-NET uses fewer training parameters and is quicker to focalize.

This provides the capability of an unsupervised layer in a multi-level structure that is automatically chosen for other illustrations. When the neural network is trained, Deep convolutional (CNN) model of decoders [19] mainly abstains the harshness of prejudice that canaries exhibit (without pre-initialization). In order to insert scientific information (such as the patient's age and weight) into the 3D U-NET formula, a total of 563 patients' data were collected and anonymized. The use of modern methods for DICOM and other medical imaging sources has showed an impressive performance in the area of morphology identification in radiography.

Additionally, the authors define the characteristic segment as x and the concatenated as x', respectively. The stacked layer corresponds to another F(x') cartography. The underlying H(x') is defined as follows:

$$H(x') = \mathrm{F}(\mathrm{x}') + \mathrm{x} \quad (1)$$

A linear projection Ws is carried out during skip connections where x and F dimensions must both be equal. The definition of the building block used is:

$$y = F(x', Wi) + Ws \quad (2)$$

The transmitter and receiver parameters of the construction block under consideration are x' and y, respectively. The function F(x', Wi) is used to express the residual mapping that needs to be learned.

The computational calculation for the 2D combination process as following:

$$\mathrm{C}(\mathrm{I} \times \mathrm{S})\mathrm{ij} = \sum_{\mathrm{m}=0}^{\mathrm{p}-1} \sum_{\mathrm{n}=0}^{\mathrm{q}-1} [\mathrm{S}(\mathrm{m}, \mathrm{n}) \times \mathrm{I}(i + \mathrm{m}), (\mathrm{j} + \mathrm{n})] + \mathrm{b} \quad (3)$$

While C denotes the yield of the fully connected layer and (i, j)denote the input ROI of the CT SCAN measurement, which ranges from 0 to 255 escalated values and the (m, n) gives the matrix measurement, where I is the characteristic outline, S is the skip of the encoder-decoder and q have an impact on the spatial assessment of the filter. The word "predisposition" is represented by b. This data is subjected to the multilayer process and the max-pooling is then attached.

Equation is used to carry out comparable feature extraction in the remaining squares of the encoder.

During training, the model assessed its performance using the Weighted Binary Cross-Entropy, loss function J, and the stochastic gradient descent optimization procedure. A better model is indicated by a greater loss function value, whereas a better training result is shown by a lower loss function value, which improved the model's performance by reducing the classification error brought on by the class imbalance between the target and background pixels.

$$J = -\frac{1}{M}\sum_{m=1}^{M} [wxym\log(h(xm)) + (1-ym)xlog(1-h(xm))] \quad (4)$$

Where M is the total number of training examples, w denotes weight, y denotes the targeted term for training case M, x denotes input image and h denotes the model's stacked neural network.

C. Post Processing Procedure of 3D Lung Cancer Slices

The post processing organization of the U-NET 3D segmentation was outlined to guarantee a forecast of 3D slices. As presented in Fig. 5, the post processing step consists of three lower stages:

- The split yield is filtered to remove the genuine positives.
- Recreation of the 2D slices from the fragmented 2D ROIs (converting 2D complete images to 2D ROI images).
- Fig. 5 shows the reconstruction of the 3D proportions from the 2D replicated slices (from 2D proportioned cuts to 3D CT SCAN) to obtain in the output the 3D U-NET segmentation.

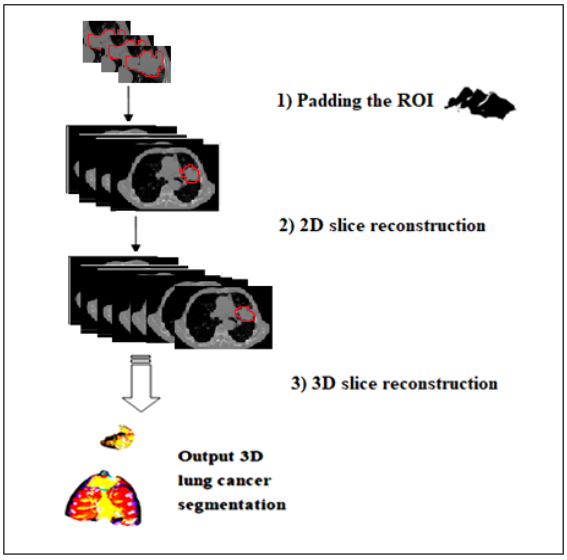

Fig. 5. The post processing step including the reconstruction of the 3D slices. (1) The padding ROI. (2) 2D slice reconstruction. (3) 3D slice reconstruction.

However, there was noise within the ROI causing the segmentation to dismount one identifier by few base pixels. There were two methods used to present the outflow of falsely positive results:

- Instead, every neuron has the attribute "1" on it.
- The erroneous positive pixels inside the quasi being suggested to be identified and removed.

The non-locale was chosen by a rectangular framework of (96×128) per each slice while considering the ROI. While pixels have been supposed to appear in the cleared-out and right areas, the authors implemented a filter to eliminate additional pixels outside of the boundaries. Then, using padding the 2D sectioned slices were restored to their distinct size of (256×256)as seen in Fig. 5. Defining every ROI in this arrangement may therefore be sliced. Finally, the 3D CT SCAN lung for each participant was rebuilt using all the clarified division. There may be a difference in the number of divisions. As a consequence, the initial slices got swapped to reconstruct the 3D lung.

III. Simulation Results

In this part, several biomedical results obtained by the proposed method are provided. Fig. 6 presents the samples of the DICOM features extracted with various CT SCAN layers.

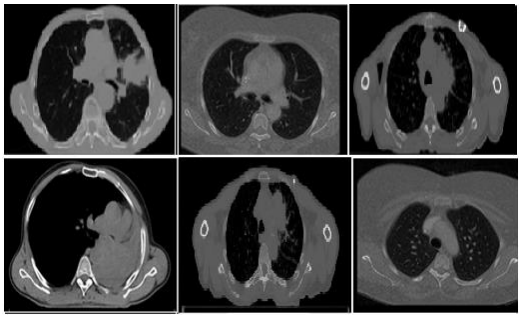

Fig. 6. Training set chosen for the scientific study.

A. Evaluation of the Results

The mean squared error (MSE) is the best and most widely utilized difference degree for image quality investigation. The MSE is easy to compute and incorporates several alluring properties applications. Moreover, it endures from a few principal issues [20] presented by the following expression (5):

$$MSE = \frac{1}{MN}\sum_{i=1}^{M}\sum_{j=1}^{N}[p(i,j) - q(i,j)]^2 \quad (5)$$

The proportion between the greatest conceivable controls of 3D images through compression of the undermining that creates distortion. The small esteem of the Peak Signal to Noise Ratio (PSNR) implies that pictures are of destitute quality. The value of PSNR for superior picture quality can be calculated based on the following equation:

$$\text{PSNR} = 10\log\frac{(2^n-1)^2}{\text{MSE}} \quad (6)$$

It should be noted that the reduced PSNR values reflect inferior cloning. On the other hand, a lower regard for MSE seems to indicate improved regeneration.

B. The Contribution Results

The encoder-decoder and primarily several varieties of completely convolution neuronal networks are marked by the U-NET layout. The class of neural network models (FCN) by integrating the interactions comprises the layer works and blocking straight to factor in the overall in the heterogeneity stage. The feature extraction draws just on fully convolution framework and is integrated with the pixel identification.

The application of the 3D U-NET Automated system applied on 3D approaches is the empirical tests dedicated to the identification of biomedical cancerology images. Fig. 7 depicts the outcomes of the segmentation of the samples [21].

Besides, TP, TN, FN, and FP successively the proportion of cancerology patches are true positive, true negative, false negative and false positive, correspondingly.

- True Positive (TP) called sensitivity: The region of crossing point between Ground Truth (GT) and division mask(S), numerically, usually coherent AND operation of GT and S.

$$\mathrm{TP} = \mathrm{GT}.\mathrm{S} \tag{7}$$

- True Negative (TN) called specificity: Equivalent to a true positive, a true negative is an ending when the classifier is trained the negative subclass with accuracy.

$$TN = 1 - \mathrm{FP} \tag{8}$$

- False Positive (FP): The anticipated zone exterior the ground truth. Usually, the coherent OR of GT and division short GT.

$$\mathrm{FP} = (\mathrm{GT} + \mathrm{S}) - \mathrm{GT} \tag{9}$$

- False negative (FN): number of pixels within the ROI zone that the model failed to anticipate. This is often the coherent OR of GT and division short S.

$$FN = (GT + S) - S \tag{10}$$

The IoU is the proportion to the combined ROI and scientific facts. Due to the parameters of TP, FP, and FN are nothing but ranges or number of pixels; ready to compose as takes after.

The anticipated ground-truth is drawn see Fig. 9 to 12, Computing Crossing point over Union can in this manner be decided through the equation below see (11):

$$\mathrm{IoU} = \frac{\mathrm{TP}}{\mathrm{TP+FP+FN}} \tag{11}$$

The performance of the research of lung cancer segmentation scheme was evaluated referring to the evaluation in the literature, namely accuracy, sensitivity, precision and dice. Those were evaluated using equations (12) to (15):

$$Accuracy = \frac{\mathrm{TP} + \mathrm{T}N}{\mathrm{TP} + \mathrm{TN} + \mathrm{FN} + \mathrm{FP}} \tag{12}$$

$$\mathrm{Sensitivity} = \frac{\mathrm{T}P}{\mathrm{TP+FN}} \tag{13}$$

$$\mathrm{Precision} = \frac{\mathrm{T}P}{\mathrm{TP+FP}} \tag{14}$$

$$\mathrm{Dice} = \frac{\mathrm{TP+TP}}{\mathrm{TP+TP+FP+FN}} \tag{15}$$

TABLE I. COMPARED THE PERFORMANCE OF THE INVESTIGATION EMPLOYING ELECTED AND CURRENTLY USED METHODOLOGIES

Methods	Name of dataset	Model	Accuracy %	Sensitivity %
The Proposed Method	Hospital	3 U-NET	98.9	97.99
Mundher AL-Shabi [11]	LIDC-IDRI	3D U-NET	95.28	94.33
Monkam and al[10]	LIDC–IDRI	3D CNN	88.28	83.82
SiyuanTang[12]	LUNA 16	3D U-NET	94	92.4

Table I indicates the accurate feature extraction rate of the database obtained inside the various experiment methods with consideration to the sensitivity and the accuracy. The medical teams appointed to accomplish the finding model as depicted in the graphic (Fig. 7). Fig. 12 demonstrates the Dice findings and the best outcomes from the contributing experiment.

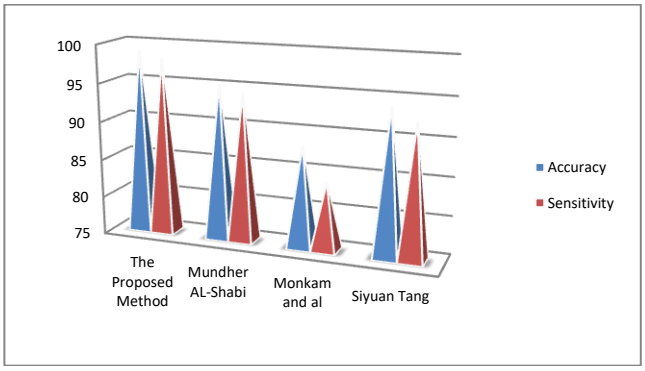

Fig. 7. Evaluation of the performance of the metrics of the sensitivity and accuracy of the proposed method comparing with other study.

As is apparent from the same, the accuracy corresponds to 88.28%, 94%, 95.28% and 98.9% of intensity values for the techniques of roughly Mundher AL-Shabi [11], Siyuan Tang [12], and the predicted model that was combined. In addition, the sensitivity corresponds to 83.82% for the methods of Monkam and al [10], 94.33% for the approaches of Mundher AL-Shabi [11], 92.4% for the algorithms of Siyuan Tang [12] and 97.99% for the processes.

Meanwhile, the malignant locations are successfully delineated in Fig. 9 and 12 utilizing the DICOM dataset; the accuracy and sensitivity were more well-liked and validated by doctors. This data will be shared in the subsequent steps.

The representative ROC curve seen in Fig. 8 was conspired to show how the algorithm can discern in mid the true positives and negatives rate. The authors will calculate the AUC "Area under the ROC Curve" which tells us how much of the plot is found beneath the curve. The closer AUC is to 1, the superior is the model. From the plot that can see the taking after AUC

measurements for each model: AUC of the calculated relapse present: The logistic regression model on the following representation of the ROC curve is demonstrated with the blue line at (0.4; 0.82) and the gradient model is presented with the orange line that held (0.1; 0.9897). The performance of the ROC curve that it grips the peak of the angle of the scheme best is the model chosen for the data segmentation.

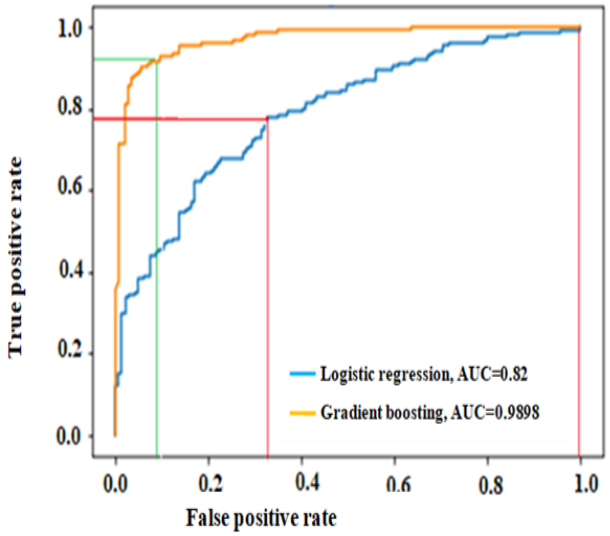

Fig. 8. The precision of the data's ROC curve presenting the false positive rate and the true positive rate presented with the logistic regression and the gradient model.

The database extracted exceeds more than 3000 slices (see Fig. 9 and 12), in 2D slices each of which are of a resolution (512×512) whose medical staff provided us their marking of each that the cases studied with the tumor dimension which is >3cm ,shown by the Tables II and III below, Through a clinical study, it was noticed that the majority of the cases present a very short life expectancy of no more than 2 years, as well as the rapid evolution of the cancer disease that reaches in a few months without any treatment the case of metastasis spreading through the bone and reaching the brain.

Due to the patient's physical and mental tiredness after undergoing surgery, chemotherapy, and radiotherapy, the treatment can be very challenging, and the severity of mortality is significant. This proves that this disease affecting this organ is responsible for breathing and the circulation of oxygen (O2) in the blood increasing the risk of a stroke.

The figures below show the marking made by the medical staff on the DICOM images. Extracted from the archiving and recording system (PACS) and the comparison with the results achieved with the segmentation systems and the proposed U-NET architecture. Fig. 9 represents the PET scan DICOM and the segmentation of the U-NET architecture compared to the (ROI) an estimate (96×128) contoured by the medical staff.

Therefore, the Dice has been employed as a loss function in the investigation. While this issue is adjusted by using probability ratios instead of Boolean, it is also known as sophisticated dice disappointment. Comparing the sophisticated dice unfortunate approach to the cross-entropy, is relatively straightforward to optimize. Analysts have frequently used the DSC equation in more recent times [22]. The DSC scoring system is used to assess the effectiveness of lung tumor segmentation. The DSC is provided in order to evaluate the outcomes of the actual and planned feature extraction (16).

$$DSC(X,Y) = \frac{2(X \cap Y)}{X+Y} \quad (16)$$

Where Y provides precise or hypothetical segmented lung regions and X relates to the predicted value of the lung segmented areas. The authors use the dice-based loss function, which is defined by (17), for assistance:

$$D = 1 - DSC \quad (17)$$

Furthermore, Fig. 9 demonstrates the segmentation of the PET scan values calculated with 90% accuracy, 91% sensitivity, and 93% dice. Where D is the delicate dice mishap, X is the ground truth, and Y is the predicted output.

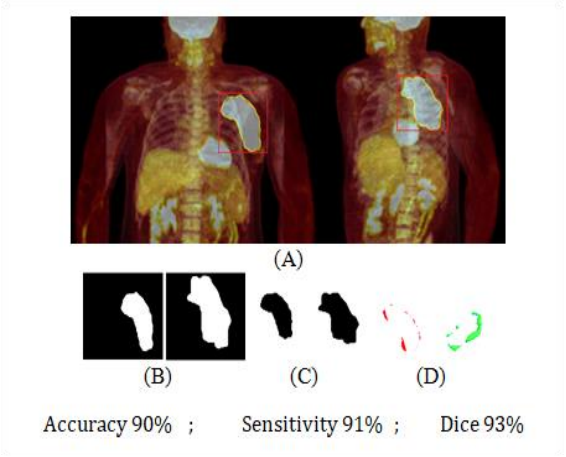

Fig. 9. Segmentation of tumors in 3D pet scan data viewed from several sides, (A) original images, (B) ROI, (C) segmentation with U-NET, (D) difference between ROI and U-NET.

The Crossing point over union is an assessment metric utilized to measure the degree of precision on a specific dataset [23]. The IoU is the essential metric to assess and demonstrate accuracy in the case of image Division. The zone of the ROI is not essentially rectangular. It can have any standard or unpredictable shape. Meaning the forecasts are division veils and not bounding boxes. In this manner, pixel-by-pixel examination is done here.

The representation of 3D medical with the ground truth of the medical staff is shown in figure (A) and (B) from Fig. 10.

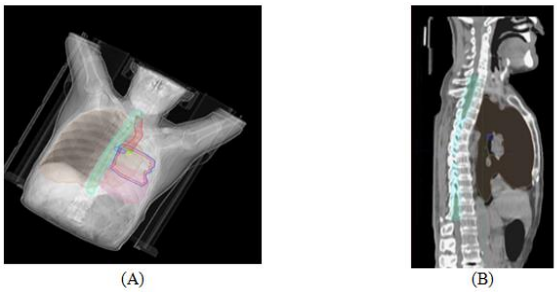

Fig. 10. 3D representation of the patient (A) and profile representation in (B).

After choosing the adequate representation from the DICOM, the second step is to upload the chosen DICOM Data of the three patients into the appropriate U-NET architecture the following 2D segmentation from the U-NET and the difference of the ROI showed in Fig. 11 that the three patients presented with 90%, 91% and 92% of accuracy, 90%, 93% and 94% of sensitivity and 91%, 92% and 95% of Dice.

The following Fig. 11 presents real cases attacked by lung cancer disease. The doctor then needs to apply margin of sub-chemical tissue to produce the clinical target volume (CTV). The margins are applied to the gross tumor volume (GTV), which is depicted in red, denotes the macroscopic, radiological measurable tumor that was selected from the appropriate software of the Eclipse contouring. Actually, it might be difficult to distinguish tumors from lung tissue in CT images. The algorithms that enable co-registration of diagnostic images with the principal simulation CT scan have been created in order to increase the accuracy of GTV identification. When comparing MRI to CT imaging for lung tumors, it reveals higher resolution and more soft tissue contrast. The clinical target volume (CTV) which is colored in orange is a second volume added to the GTV as a margin to cover nearby locations that must be targeted in order to cure disease that could be present at microscopic levels. Based on anatomical and ROI data obtained from cross-sectional imaging, the CTV is defined. Uncertainty in treating is accommodated by the geometrical software of the planned target volume (PTV) bounded with blue hue, it accounts for the daily random and systematic fluctuations in patient setup, additionally to the internal motion of the tumor during treatment (internal target volume (ITV) displayed in green).These variations may include shifts in the tumor's position and shape as a result of its regression or growth, bladder filling or rectal distension, as well as, unforeseen changes brought on by a change in the patient's position or the method used to set up the machine between each delivered fraction. As a result, the PTV is the suggested parameter to ensure that all areas of the CTV areas receive an acceptable dose of radiation.

When looking at the planning of the non-small cell lung carcinoma patient in the 3D, the software reconstructs the data in sagittal and coronal planes. That helps the doctors to plan the volumes in 3D by the contouring then the doctors use the lung window that is easier to visualize the extend of the volume tumor. Then the pitch that present the distance travelled in one 360° rotation in the CT Scan, remaining the breathing during treatment with the same parameters see (18) and (19).

After uploading the different parts of the slices from different representation the second step consists of choosing one of the best results that are the adequate representations, and to do the 3D image representation from the 2D and try to have the final 3D result of the best-case result with 92% of accuracy, 94% of sensitivity and 95% of dice, see Fig. 12.

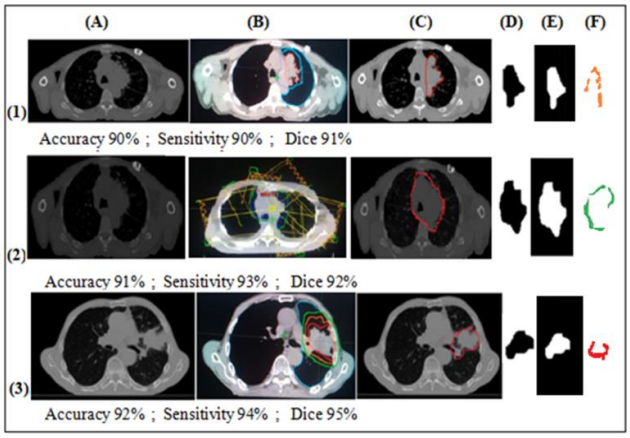

Fig. 11. Segmentation 3D of lungs seen from DICOM;(A) original image;(B) predicted 3D image by medical staff;(C) ground truth mask;(D) segmentation with U-net; (E)ROI;(F)difference between ROI and U-NET.

The results confirm the similarity between the extraction of the volume parameters and surface measured from the different slices (S1, S2, S3 and S4) with the ground truth (cm^2) compared with medical staff estimation volume (cm^3) see Table II:

TABLE II. VOLUME OF CANCER IN RELATION TO TOTAL LUNG VOLUME EXTRACTED WITH MEDICAL STAFF

N° Patient	Volume cancer (cm^3)	Volume of the normal lung (cm^3)	Volume two lungs (cm^3)
1	541	2500	4459
2	540	1855	3170
3	112	927	1742

The result of the extracted ROI results from U-NET architecture with the choice of the third patient as best case result, see Table III and the following equation:

TABLE III. VOLUME OF THE LUNG CANCER EXTRACTED FROM THE U-NET ARCHITECTURE OF FIG. 11 BEST CASE OF THE THIRD PATIENT

	S1	S2	S3	S4
Surface (cm^2)	31.737	54.088	15.945	9.40
Volume (cm^3)		111.17		

$$CTV = GTV + the\ pitch \quad (18)$$

$$PTV = CTV + the\ pitch \quad (19)$$

After presenting the best case results of Tables II and III of the third patient the authors will choose the best slices from the parameters of accuracy, sensitivity and dice of the showed results in Table III and II and Fig. 11 and upload it into the U-NET architecture to finally obtain the 2D segmentation of the different slices and the 3D representation of the ROI segmentation of the best result communicated in Table I and compared with other authors that are demonstrated (see Fig. 12) and present the best accuracy 98.9%, sensitivity 97.99% and dice 97%, that explained the segmentation of 3D lungs seen from DICOM.

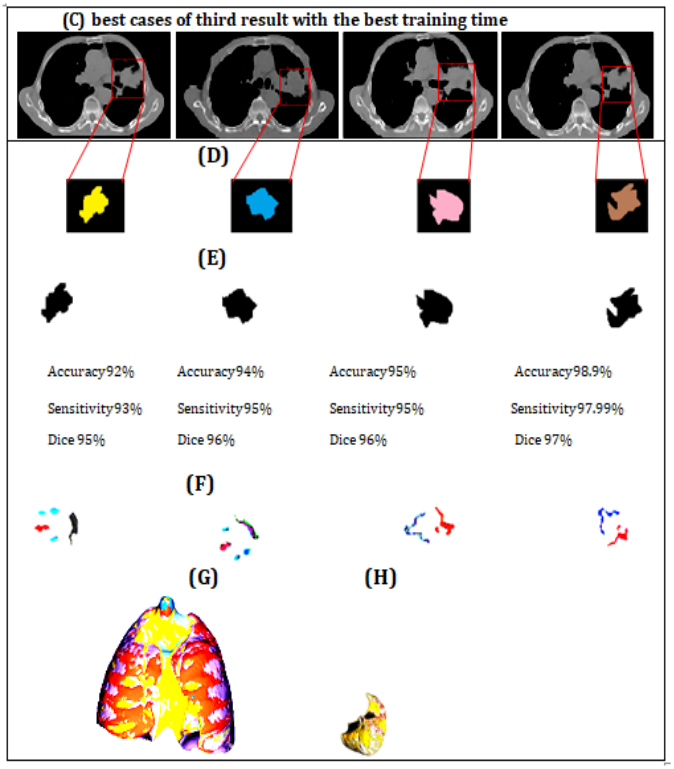

Fig. 12. Segmentation 3D of lungs seen from DICOM, (A) original image, (B) predicted 3D image by medical staff, (C) ROI with ground truth mask, (D) ROI, (E) segmentation with U-net, (F) concatenated 3D images between (E) and (D), (H) and (G) 3D lung segmentation.

Interestingly, in accordance with the 3D U-NET architecture's empirical offshoots seen in Fig. 12, the recommended procedure is more accurate than the conventional framework in terms of delineation performance, as evidenced by the segmentation's sensitivity [24] for further data, seen in Table I.

C. Generating the Luminosity Picture of the Data

Images captured using specular microscopy typically has low contrast and non-uniform illumination throughout. Here, we want to determine whether picture improvement for CNN would be beneficial. Standardizing the fourth result of the output images in Fig. 12 is also a typical procedure in neural networks. We suggested using contrast constrained adaptive histogram equalization with a kernel of (96×128) to improve local image contrast.Where In present the norm of the image I(X,X') and this kernel size roughly correspond to the size of an average cell see 20.

$$In(X,X') = \frac{\mathrm{I(X,X')} - \min(\mathrm{I(X,X')})}{\max(\mathrm{I(X,X')}) - \min(\mathrm{I(X,X')})} \quad (20)$$

The advantages of local contrast enhancement would be diminished by a kernel that is too large, while noise would be excessively amplified by a kernel that is smaller than half of a cell. We found that intensity normalization significantly improved performance see Fig. 13.

Interestingly, in accordance with the 3D U-NET architecture's empirical offshoots, the recommended procedure is more accurate than the conventional framework in terms of delineation performance, as evidenced by the segmentation's sensitivity [24].For further data, see Table I. Furthermore, the split sensitivity treatment in the database presented in Fig. 13 seems to be more important compared to any other recommended approach. This indicates that, in comparison to the various ways that have been exhibited, the addition of 3D U-NET can help networks achieve the highest execution of the concept of three - dimensional segment.

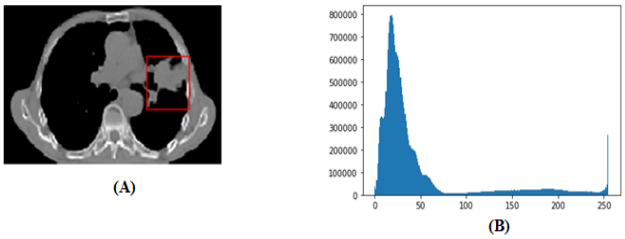

Fig. 13. Redistribution of the histogram of the result of (A) by intensities shifts (B) of the data.

Furthermore, the split sensitivity treatment in the database presented in Fig. 13 seems to be more important compared to any other recommended approach. This indicates that, in comparison to the various ways that have been exhibited, the addition of 3D U-NET can help networks achieve the highest execution of the concept of three - dimensional segment.

This paper relates the outputs of the consecutive frames depicted in Section 3 to evaluate the allocation grey level approaches in the histogram and its establishment. The first two items featured in the original imagery on which the juxtaposition was done may be clearly distinguished [25]. The other two photos display the intensity value adjustment's dispersion in relation to the original imagery. Variance is utilized as a criterion among the gray scale images' cohesiveness [26] that are formed via numerous 3D imagery of (512×512) pixels, once data experimentation has been authenticated. To enable the clinician to fine-tune his diagnosis, the objective is to segment the specific area of interest the (ROI) an estimate (96×128) contoured by the medical staff. Accordingly, the identification must be exact around the subject of interest and must not be hampered by imaging interference (such as patient movement or perspiration).

The consequence allows for a degree of robustness to variations in average luminance by treating the histogram as a compactness of likelihood (probability and impact of a grey scale similar level to all the pixels).

The progress of the diagram demonstrates that the selected assumption may be true since the concluding the artifact setting that nearly equal to Gaussian. These values were as opposed to those created since the epochs by trying to minimize the variance and by reducing the fluctuation threshold, where the disparity of the Gaussian function is predicted in every incarnation of the dataset.

The statistical likelihood p of the intensity of the histogram distribution, together with its mean μ and the variance σ^2 shown in (21):

$$p = \frac{1}{\sqrt{2\pi\sigma^2}} e^{(-\frac{(X-\mu)^2}{2\sigma^2})} \quad (21)$$

The predicted linear growth in the histograms results in a broader range of gray levels for the main image. As seen by the outcomes in Fig. 13, the performance of the histogram segmentation in PETSCAN and CT SCAN data presented in 3D medical imaging and proved with the results of the pixels intensity are determinate; that can prove that the implementation on the U-NET architecture is more sufficient compared to other literature which concentrates on one study. This contribution opens horizon to data scientists to develop their research with the cooperation of medical staff to obtain the best result in little time and reduce the exposition on x-ray that can have a bad effect especially on the patient.

IV. Discussion

The new proposal incorporates a modern sequence segmented technique on the U-NET Algorithm, compared to the result of other data performs the contouring and the final vision of medical staff that the result of the research was achieved and applied with different data from different service unlike other literature applied to a single and unspecified one. This study is the first to discern the importance of deep science in the medical field, especially in 3D image detection. This way offers the chance to develop other perspectives in the near future.

First of all, the 3D segmentation predicting necessitates significantly more complicated computational resources, which in turn affects a model's capacity to execute the training with huge datasets [27]. According to certain research, 2D U-Net performed more accurately, consumed less memory, and required less training time than 3D U-Net. Instead of a 3D segmentation model, several 2D segmentation models targeting the 3D segmentation in U-NET were created. By combining the 2D segmentation model with modern pre- and post-processing image evaluation techniques, researchers were able to build the U-NET, a completely automated end-to-end 3D segmentation network. So, compared to other systems, U-NET provided us with a better performance using the real data extracted from Salah Azaiez Institute.

Secondly, considering its small morphology and constrained location decisions, CT scan is considerably harder for segmentation effectively than other work structures that are frequently segmented manually. The difficult task of segmenting is resolved in this study by the U-NET approach and enhanced image analysis techniques. The comparative examination demonstrates the ability to segment skills of the U-NET. The research's findings and its comparison with previous studies have highlighted the U-NET advantages. As far as the authors are aware, the automatic end-to-end 3D segmentation findings are state-of-the-art [28]. The current study showed that the U-NET technique has considerable potential for creating an automatic and precise segmentation tool for extremely difficult medical imaging segmentation challenges [29].

As 3D U-NET architecture can still be improved, but the authors need an innovative method to solve a difficult segmentation issue like the subject matter and incompatibility problem.

V. Conclusion

The suggested approach entails developing a new scientific perspective for the biomedical industry through networking, which improves credible steps in radiation healthcare, notably for tumor segment diagnostics.

The acquired results show that these methodologies can accurately divide an image into homogenous parts and show the potential of the testing, which provides a foundation for the creation of biological data science images. The cooperative work between medical fields and scientists opens the horizon for many points, especially the hardness of the localization of the ROI and the validity of the purpose which demands such time and effort from each contributor. This work was established to perform the imaging system in the medical field of the institute of Salah Azaiez.

For further investigation the requirement for more effective ROI identification while working with various CT scan datasets. Using more sophisticated models, such attention modeling or sequential modeling using GAN for future work, the deep learning networks could be expanded to include contextual data, to overcome the paucity of human-annotated data, a semi-supervised technique involving human and machine collaboration is needed rather than supervised learning.

Acknowledgment

The technical staff provides us with the study realized in collaboration with the institute of Salah Azaiez which offers us the required materials and has a significant impact on the success of this work.

Authors' Contributions

ELLOUMI Nabila wrote the paper, slim ben CHAABANE and Hassen SEDDIK contributed to this research with technical and academic writing assistance. The final paper was read and endorsed by all writers.

Availability of Data and Materials

The DICOM images utilized in the research described in this publication were received from the Institute of Salah Azaiez of Cancerology in Tunisia and are publicly accessible for use in the public's research. The District Referral Hospital will use the tool, which is still in the process of being tested.

Financial Support and Sponsorship

Not Applicable.

Conflicts of Interest

Not Applicable.

Ethical Approval and Consent to Participate

Since this was a registration-only study, the ethics reviews board accepted it for release without requesting informed consent from research participants.

REFERENCES

[1] A.Ben Slama, Zbarki, H.seddik, J.Marrakchi, S. Boukriba, Salam Labidi" Improving Parotid Gland Tumor Segmentation and Classification Using Geometric Active Contour Model and Deep Neural Network Framework",InternationalInformation and Engineering Technology Association ,2021[DOI: 10.18280/ts.380405]

[2] Z.Mbarki,A.Ben Slama,H.Seddik,H.Trabelsi, " Building a smart dynamic kernel with compact support based on deep neural network for efficient X-ray image denoising", TCIV, Computer Methods in Biomechanics and Biomedical Engineering: Imaging & Visualization. ISSN / eISSN: 2168-1163 / 2168-1171 2021,[DOI: 1080/21681163.2021.1987331]

[3] A.BenSlama,Z.Mbarki,H.Seddik,J.Marrakchi,S.Boukriba,S.Labidi, "Improving Parotid Gland Tumor Segmentation and Classification Using Geometric Active Contour Model and Deep Neural Network Framework" Traitement du Signal,2021, Vol. 38 Issue 4, p955-965. 11p

[4] S.Bachir"Elaboration d'un modèle quantitatif pour la discrimination des cellules tumorale selon le facteur Ki67", génie électrique, « ATSIP », 2015

[5] Slim Ben Chaabane, HasseneSeddik and Rafika Harrabi, " Face recognition based on statistical features and SVM Classifier", Multimedia Tools and Application Journal, ISSN 1573-7721, 81, pages8767–8784 (5 February 2022)

[6] FunaZhou , Zhiqiang Zhang , Sijie Li Research on federated learning method for fault diagnosis in multiple working conditions. Complex Engineering Systems 2021[DOI: 10.20517/ces.2021.08]

[7] ZhaominLv Online monitoring of batch processes combining subspace design of latent variables with support vector data description. Complex Eng Syst 2021[DOI: 10.20517/ces.2021.02]

[8] Slim Ben Chaabane, HasseneSeddik and Rafika Harrabi, " Face recognition based on statistical features and SVM Classifier", Multimedia Tools and Application Journal, ISSN 1573-7721, 81, pages8767–8784 (5 February 2022)

[9] Mohamed ben gharsallah and Hassene SEDDIK, "Phase congruency-based filtering approach combined with a convolutional network for lung CT image analysis", The imaging science Journal, Received 22 May 2020, Accepted 12 Dec 2022, Published online: 02 Jan 2023, [DOI: 10.1080/13682199.2022.2159291]

[10] ImenLabiadh, Hassene Seddik, Larbi Boubchir, "Deep Learning for Detection of Prostate Tumors by Microscopic Cells and MRI", 6th International Conference on Advanced Technologies for Signal and Image Processing, ATSIP, 10.1109 / 9805866, IEEE Xplore, No 21844743, 2022.

[11] Monkam P, Qi S, Xu M, Han F, Zhao X, Qian W (2018) CNN models discriminating between pulmonary micro-nodules and nonnodules from CT images. BioMed EngOnLine 17(1):96.[doi.org/10.1186/s12938-018-0529-x]

[12] Mundher Al-Shabia ,Kelvin Shaka ,Maxine Tana,b(2022),"ProCAN: Progressive Growing Channel Attentive NonLocal Network for Lung Nodule Classification",PatternRecognition,ELSEVIER,[DOI:10.1016/j.patcog.2021.108309]

[13] Siyuan Tang, Min Yang, JinniuBai,(2020) ; "Detection of pulmonary nodules based on a multiscale feature 3D U-NET convolutional neural network of transfer learning. PLoS ONE "15(8), 2020 .[DOI:10.1371/journal.pone.0235672]

[14] Mundher AL-Shabi, Wei Chen ,andYusong Tan ;Point-Sampling Method Based on 3D U-NET Architecture to Reduce the Influence of False Positive and Solve Boundary Blur Problem in 3D CT Image Segmentation,2020[DOI: 10.3390/app10196838]

[15] Detection of pulmonary nodules based on a multiscale feature 3D U-NET convolutional neural network of transfer learning, PLoS ONE 15(8),2020. [DOI: 10.1371/journal.pone.0235672]

[16] O. Ronneberger, P. Fischer, and T. Brox, "U-net: Convolutional networks for biomedical image segmentation," in International Conference on Medical image computing and computer-assisted intervention. Springer, 2015, pp. 234– 241.[DOI: 10.48550/arXiv.1505.04597]

[17] Glorot X, Bordes A, Bengio Y (2011) Deep sparse rectifer neural networks. In: Proceedings of the fourteenth international conference on artifcial intelligence and statistics, pp 315–323

[18] Wan L, Zeiler M, Zhang S, Le Cun Y, Fergus R (2013) Regularization of neural networks using dropconnect. In: International conference on machine learning, pp 1058–106

[19] J. Fu, J. Liu, H. Tian, Y. Li, Y. Bao, Z. Fang, and H. Lu, "Dual attention network for scene segmentation," pp. 3146– 3154, 2019. [DOI:10.3390/s22124477]

[20] Detection of pulmonary nodules based on a multiscale feature 3D U-NET convolutional neural network of transfer learning. PLoS ONE 15(8), 2020 .[DOI:10.1371/journal.pone.0235672]

[21] X. Li, Q. Dou, H. Chen, C.-W. Fu, X. Qi, D. L. Belavy,` G. Armbrecht, D. Felsenberg, G. Zheng, and P.-A. Heng, "3d multi-scale fcn with random modality voxel dropout learning for intervertebral disc localization and segmentation from multi-modality mr images," Medical image analysis, vol. 45, pp. 41–54, 2018. [DOI: 10.1016/j.media.2018.01.004].

[22] Xu M, Qi S, Yue Y, Teng Y, Xu L, Yao Y, et al. Segmentation of lung parenchyma in CT images using CNN trained with the clustering algorithm generated dataset. Biomed Eng Online 2019[http://dx.doi.org/10.1186/s12938-018-0619-9]

[23] S. Bakas, M. Reyes, A. Jakab, S. Bauer, M. Rempfler, A. Crimi, R. T. Shinohara, C. Berger, S. M. Ha, M. Rozycki et al, "Identifying the best machine learning algorithms for brain tumor segmentation, progression assessment, and overall survival prediction in the brats challenge," arXiv preprint arXiv:1811.02629, 2018.[DOI: 10.48550/arXiv.1811.02629].

[24] J. Fu, J. Liu, H. Tian, Y. Li, Y. Bao, Z. Fang, and H. Lu, "Dual attention network for scene segmentation," pp. 3146– 3154, 2019. [DOI:10.48550/arXiv.1809.02983]

[25] Kermany, D.; Zhang, K.; Goldbaum, M. Labeled optical coherence tomography (oct) and chest X-ray images for classification. Mendeley Data 2018[DOI: 10.17632/rscbjbr9sj.2]

[26] Liang, G.; Zheng, L. A transfer learning method with deep residual network for pediatric pneumonia diagnosis. Comput. Methods Programs Biomed. 2020, 187, 104964[DOI: 10.1016/j.cmpb.2019.06.023]

[27] Ibrahim, A.U.; Ozsoz, M.; Serte, S.; Al-Turjman, F.; Yakoi, P.S. Pneumonia classification using deep learning from chest X-ray images during COVID-19. Cogn. Comput. 2021, 1–13.[DOI: 10.1007/s12559-020-09787-5]

[28] Bahar U.M; Guan Y.H; Abdullah A.M; Em P.P; Qingliu W." Deep Learning-Based Segmentation of 3D Volumetric Image and Microstructural Analysis".Sensors 2023.[DOI: 10.3390/s23052640]

[29] Xiang .L; Zhaonan .S; Chao.H; Yingpu. C; Jiahao .H; Xiangpeng .W; Xiaodong Z; Xiaoying W" Development and validation of the 3D U-Net algorithm for segmentation of pelvic lymph nodes on difusion-weighted images"BMC Medical Imaging 2021[DOI:10.1186/s12880-021-00703-3